Spatial distribution of venous gas emboli in the lungs

JENNIFER E. SOUDERS,[1,2] JEFFREY B. DOSHIER,[1]
NAYAK L. POLISSAR,[4] AND MICHAEL P. HLASTALA[1,3]
Departments of [1]Medicine, [2]Anesthesiology, and [3]Physiology and Biophysics, University of Washington, Seattle 98195-6522; and [4]The Mountain-Whisper-Light Statistical Consulting, Seattle, Washington 98105

Souders, Jennifer E., Jeffrey B. Doshier, Nayak L. Polissar, and Michael P. Hlastala. Spatial distribution of venous gas emboli in the lungs. *J. Appl. Physiol.* 87(5): 1937–1947, 1999.—The distribution of gaseous pulmonary emboli is presumed to be determined by their buoyancy. We hypothesized that regional pulmonary blood flow may also influence their distribution. Therefore, pulmonary blood flow was measured in supine, anesthetized dogs with use of 15-μm fluorescent microspheres at baseline and during N_2 embolism. The animals were killed, and the lungs were excised, air-dried, and diced into ~2-cm^3 pieces with weights and spatial coordinates recorded. Embolism was defined as a >10% flow decrease relative to baseline. Vertically, the incidence of embolism increased substantially by 6 ± 1% per additional centimeter in height compared with baseline (P = 0.0003). Embolism also increased radially by 3 ± 1%/cm from the hilum (P = 0.002). There was a weaker but statistically significant increase in embolism to pieces with greater baseline flow, 9 ± 2% for every 1.0 increase in relative baseline flow (P = 0.008). We conclude that the distribution of gaseous emboli is influenced by buoyancy and flow dynamics within the pulmonary vasculature.

fluorescent microspheres; air embolism; pulmonary gas exchange; pulmonary circulation; decompression illness

PULMONARY AIR EMBOLISM has been a subject of interest to clinicians and researchers for many years because of the severe hemodynamic and gas exchange abnormalities that result (29). Many studies of pulmonary air embolism have been done in the context of decompression illness, which is a prominent problem for divers (43) but may affect aviators and astronauts as well (36, 47). Victims can be devoid of pain or other symptoms, even with concomitant extrapulmonary embolism. Pulmonary air embolism is also known to occur during surgical procedures and traumatic injuries and has been demonstrated to cause elevated pulmonary arterial pressure, elevated systemic arterial pressure, elevated pulmonary vascular resistance, reduced cardiac output, systemic hypoxia, and systemic hypercarbia (12, 13, 35, 44). It is the N_2 in the air that is responsible for these effects.

When air bubbles enter the venous blood, they are carried to the right heart and undergo turbulent mixing and disruption in the right ventricle. If the bubbles are not of sufficient size to obstruct the right ventricular outflow tract, they will be ejected into the pulmonary arteries, possibly after being decreased further in size as a result of right ventricular mixing. The emboli travel through the pulmonary vessels and are trapped in the small arterioles and capillaries (1, 35, 37), with almost no further passage into the left heart and systemic circulation (6, 7). Little is known about where the bubbles distribute after leaving the right heart and the dynamics of their resorption over time.

In prior studies of the gas exchange abnormalities associated with pulmonary air embolism (27, 48), it was shown that there was no increase in dead space ventilation with N_2 embolism, despite the obstruction of the pulmonary vessels. Instead, there was an increase in the lung regions with high ventilation-to-perfusion ratios ($\dot{V}_A/\dot{Q}$) and also an increase in areas with low $\dot{V}_A/\dot{Q}$. Presumably, the pulmonary blood flow (PBF) redistributed to lung regions where the pulmonary vessels were not blocked with bubbles, and these regions then became relatively overperfused and underventilated. This increased $\dot{V}_A/\dot{Q}$ heterogeneity is likely responsible for the hypoxia and hypercarbia that result when air embolism occurs. The gas exchange abnormalities were no longer present 30 min after the cessation of embolism, indicating that the emboli had completely resorbed or were not present in sufficient size or quantity to cause $\dot{V}_A/\dot{Q}$ aberrations.

Two other studies have looked at the actual distribution of air emboli in the lung vasculature. In the first study, dogs were studied in the prone and supine positions, and the emboli were tracked using a radioactive xenon tracer method (10). In the second study, physical models of the pulmonary vessels were employed to observe how the bubbles might behave at bifurcations and when lodging in small arterioles and capillaries (11). In both studies it was concluded that the buoyancy of bubbles would be the primary determinant of their distribution; i.e., the bubbles would always float to the top. In addition, it was concluded that >20- to 30-μm bubbles would not pass through to the systemic circulation. However, there is a problem with the radioactive xenon method, because it is limited in its resolution and requires the investigator to look only in the plane of PBF distribution that will presumably be affected. We hoped to obtain more information about the distribution of the emboli in other spatial dimensions. In addition, we wanted to know whether the initial magnitude of blood flow in a pulmonary vessel increased the incidence of embolization to that vessel, irrespective of its spatial position in the lung. We

The costs of publication of this article were defrayed in part by the payment of page charges. The article must therefore be hereby marked "*advertisement*" in accordance with 18 U.S.C. Section 1734 solely to indicate this fact.

theorized that dynamic factors such as the release of inflammatory mediators or hypoxic pulmonary vasoconstriction could have additional effects on the distribution of bubbles lodging in the pulmonary vessels.

The purpose of this study, therefore, was to study the three-dimensional distribution of PBF on a finer scale of resolution before, during, and after venous embolism with N_2 in an intact animal model. We hoped to shed more light on the interactions between buoyancy and flow in determining bubble location.

MATERIALS AND METHODS

After approval of the experimental protocol by the Animal Care Committee of the University of Washington, six mixed-breed dogs of either gender [27.0 ± 2.9 (SD) kg body wt] were studied.

Anesthesia and Instrumentation

An intravenous catheter was placed in the foreleg, and anesthesia was induced with thiopental sodium (20 mg/kg) and continued with a thiopental sodium infusion of 10–15 $mg \cdot kg^{-1} \cdot h^{-1}$ to maintain hemodynamic stability and suppress responses to any noxious stimuli. After anesthesia was induced, an oral endotracheal tube was placed, and the lungs were ventilated with atmospheric air by means of a conventional piston-pump ventilator (dual-phase respirator pump model 608, Harvard Apparatus) set for a tidal volume of 15 ml/kg. The animals were positioned supine for intubation and instrumentation and remained in the supine position for the duration of the experiment.

A large-bore femoral arterial catheter was inserted for pressure monitoring and blood sampling; it was positioned so that the tip was in the abdominal aorta just caudal to the level of the diaphragm. Bilateral femoral venous catheters were placed. One catheter was used for administration of the N_2 emboli and was positioned in the inferior vena cava so that the tip was just caudal to the level of the diaphragm. A vascular introducer sheath was placed in the other femoral vein to allow a balloon-tipped thermodilution pulmonary arterial catheter (Baxter Healthcare, Irvine, CA) to be floated into the pulmonary artery to monitor pulmonary arterial pressure, pulmonary capillary wedge pressure, blood temperature, and cardiac output. The introducer and pulmonary arterial catheter were also used to allow infusion of anesthetic drugs and maintenance fluids. An additional venous catheter was placed in one of the external jugular veins for injection of fluorescent-labeled microspheres.

Arterial blood pressure, pulmonary arterial pressure, airway pressure, and end-tidal CO_2 were measured continuously and recorded on a data-management system (Mark 12, DMS 1000, Western Graphtec) with Validyne amplifiers. Cardiac output, blood temperature, and arterial and mixed venous blood gas values were measured at conditions of steady state and under the N_2 embolism study conditions (see below). The end-tidal CO_2 was measured with a mass spectrometer (medical gas analyzer MGA-1100, Perkin-Elmer). The cardiac output and blood temperature were measured with a cardiac output computer (model Sat-2, Baxter Edwards). Arterial and venous pH, P_{O_2}, and P_{CO_2} were measured with a blood-gas analyzer (model ABL 330 Acid Base Laboratory, Radiometer, Copenhagen, Denmark) and corrected for temperature. The ventilatory rate of the lungs was adjusted to maintain the arterial P_{CO_2} at 38.8 ± 2.7 (SD) Torr.

Venous N_2 Embolism and Study Conditions

N_2 bubbles were infused into the femoral vein at a rate of 0.2 $ml \cdot kg^{-1} \cdot min^{-1}$ for 30 min with use of a constant-flow syringe infusion pump. This embolic load was sufficient to more than double the pulmonary arterial pressure after 5 min of bubble infusion. The bubbles were formed by forcing the N_2 through a PE-20 catheter, resulting in ~1.2-mm-diameter bubbles, as estimated using a stroboscopic light, as described previously (27). However, because these bubbles were allowed to be mixed in the right atrium and ventricle before entering the pulmonary artery, it is likely that the size range of the bubbles was broader as a result of this disruption. The bubbles that were initially administered could break up into smaller bubbles or coalesce into larger ones as a result of this mixing.

Because Hlastala et al. (27) had studied the gas exchange of the lungs at 15 and 30 min after initiation of embolization, we chose to study these same time periods. Therefore, arterial and venous blood-gas samples and hemodynamic measurements were taken, and fluorescent microspheres were injected at the following times: baseline, after 15 min of N_2 embolism ($N_2$15), and after 30 min of N_2 embolism ($N_2$30). In addition, hemodynamic measurements, blood samples, and a fluorescent microsphere injection were performed during the recovery phase at 15 and 30 min after the cessation of the N_2 embolism (R15 and R30, respectively).

Fluorescent Microsphere Technique

After hemodynamic measurements were taken under each study condition, samples were drawn for arterial and venous blood-gas measurements. After blood sampling, ~2–3 × 10^6 15-μm-diameter fluorescent polystyrene microspheres (FluoSpheres, Molecular Probes, Eugene, OR) were injected via the jugular venous catheter over 30 s. Before injection, the microspheres were sonicated for 2 min and then vortexed. Each injection was followed by 20 ml of normal saline flush. Five colors (red, orange, blue-green, yellow-green, and crimson) were used, with the order of the injection of the colors randomized in each experiment.

At the completion of the study, each animal was given an additional bolus of 5–7 mg/kg thiopental sodium followed by 1,000 U/kg heparin (Elkins-Sinn, Cherry Hill, NJ) and 3 mg/kg papaverine hydrochloride (YorPharm, Buffalo Grove, IL); then they were exsanguinated. The chest was opened by midline sternotomy, and catheters were placed in the main pulmonary artery and the left atrium to isolate the pulmonary circulation. The lungs were flushed free of blood with 1 liter of 2% dextran (Sigma Chemical, St. Louis, MO), removed intact, and then air-dried at total lung capacity (TLC).

The dried lungs were then positioned in a miter box so as to reproduce the isogravitational planes in vivo and were encased in polyurethane foam insulating sealant to provide a rigid orthogonal reference system. The lungs were then diced into 1.9-cm^3 pieces, and each piece was weighed and assigned *x*, *y*, and *z* coordinates. The pieces were then soaked in 2-ethoxyethyl acetate (Cellosolve acetate, Aldrich Chemical, Milwaukee, WI), and the fluorescence was read in a luminescence spectrophotometer (model LS-50B, Perkin-Elmer) fitted with a standard cuvette reader and a red-sensitive photomultiplier tube. Regional PBF for each lung piece was calculated from fluorescent microspheres data according to the methods of Glenny et al. (16). Briefly, lung pieces with abnormal appearance or with >25% airway content on visual inspection were excluded from analysis, and in the remaining pieces the weight-normalized relative PBF (WNRF) was calculated. The hilar-to-peripheral (*h*) distance was determined according to the methods of Glenny et al. (17).

Data Analysis and Statistical Methods

Descriptive statistics. Because the primary goal of our study was to try to gain more information about the interactions between buoyancy and flow on bubble location, we decided to focus our data analysis on the distribution of PBF only during the baseline and embolism ($N_2$15 and $N_2$30) conditions.

Descriptive statistics of hemodynamic parameters, spatial flow gradients, and other variables are usually presented as means ± SE calculated across the six animals. Differences in hemodynamic parameters between pairs of conditions are analyzed using the two-sided paired *t*-test ($N_2$15 vs. baseline, $N_2$30 vs. $N_2$15, and $N_2$30 vs. baseline). In all cases, $P < 0.05$ was considered statistically significant. There has been no adjustment of *P* values for multiple testing, because each *P* value addresses a comparison between states with potentially unique effects.

Effect of embolism on perfusion. The effect of N_2 embolism on perfusion is described by two variables. First, a piece of lung was considered to have substantial embolism if there was a strong enough negative effect on perfusion that a decrease of >10% in flow (relative to baseline) was observed. The 10% value is highly likely to be a nonrandom decrease and was determined as follows. Approximately 1,000 or more fluorescent microspheres were injected per piece, yielding a Poisson standard error for the average piece of ≤3% [$\approx 100\% * 1/(1{,}000)^{0.5}$]. Random time variation over 15 min in anesthetized dogs has been shown previously to be ~5% (18). Pooling these two sources of random variation yields a standard error of ~6% [$\approx(5^2 + 3^2)^{0.5}$]. Finally, on the basis of normal approximation and with the assumption of the null hypothesis of no effect of embolism, only ~5% of the pieces would have a random fluctuation decreasing the flow from baseline by >10% ($\approx 6\% * z_{0.95}$, where $z_{0.95} = 1.64$). Although there is a series of approximations here, we can be confident that the vast majority of pieces with >10% decrease in flow have lost flow because of embolism. A dichotomous variable indicating a >10% loss of flow compared with baseline (vs. a smaller loss or an increase) was therefore calculated for all pieces at $N_2$15 and, as a separate variable, for all pieces at $N_2$30.

The second type of variable describing change in flow was the simple difference in relative flows, yielding two change variables: $N_2$15 − baseline and $N_2$30 − baseline.

Influence of spatial dimensions and baseline flow on perfusion. In this study our interest focused on spatial dimensions and baseline flow as factors that would influence which pieces were affected by embolism. Spatial dimensions were defined as *x* (lateral left-to-right gradient), *y* (vertical back-to-front gradient, which is also the gravitational gradient in this study), *z* (horizontal caudal-to-cranial gradient), and *h* (the radial distance to the hilum of each lung) (17). The baseline (preembolism) flow was hypothesized as a mechanism transporting more N_2 bubbles to pieces with higher blood flow rates.

WNRF was plotted against each of the spatial dimensions of *x*, *y*, *z*, and *h*, and slopes of the relationships between flow and spatial dimension were determined using least squares regression. Changes in the slopes among the three study conditions of baseline, $N_2$15, and $N_2$30 were calculated by subtraction and compared using the single-sample *t*-test. Significant changes in regional PBF occurred only in the *y* and *h* distributions (see RESULTS). The *x* and *z* dimensions were therefore excluded from the next series of analyses.

The influence of the baseline flow on flow changes can also be described by least squares regression coefficients, analogous to the spatial dimensions *y* and *h*. Least squares regression was therefore performed for the influence of *y*, *h*, and baseline flow on the dichotomous variable indicating a >10% loss of flow. All the slope coefficients are readily interpretable. For example, if the dichotomous indicator of embolism-affected pieces is regressed on the *y* dimension, yielding a slope coefficient for *y* of 4.2, it indicates that the incidence of embolized lung pieces increases, on the average, by 4.2% for each vertical centimeter in the lung. Similarly, a coefficient of −1.4 for baseline flow when the change in flow (e.g., $N_2$15 − baseline) is regressed on baseline flow indicates that, on the average, relative flow decreases by 1.4% of the whole lung's mean relative flow when one piece has 1.0 more relative flow unit at baseline than another.

The influence of spatial dimensions and baseline flow on the location of N_2 emboli is summarized by the mean of the regression coefficients across the six animals. The null hypothesis of "no effect" was tested using the two-sided single-sample *t*-test comparing each mean regression coefficient with zero. Correlations among *y*, *h*, and baseline suggested potential confounding among these variables; therefore, regression models were calculated *1*) for each of these three variables as a single predictor, *2*) for all three of the variables as joint predictors, and *3*) in the case of baseline, which was most affected by confounding, by using the residuals of the dependent variable regressed on *y* and *h* (a step that removes linear effects of *y* and *h* on the dependent variable) and then regressing the residuals on baseline blood flow as the independent variable. The third procedure provides the most conservative estimate of the impact of baseline blood flow.

We also partitioned the total variation in flow of the combined embolism and the baseline states into two components: *1*) a fixed component due to biological structure (the position of a piece in the whole lung, or the "piece effect") and *2*) a component due to dynamic changes, where such changes include the embolism, time variation, and methodological noise (the random variation in microsphere distribution and laboratory measurements). The contribution of each source of variation, "piece" or "change," can be expressed as two percentages adding up to 100%. Details of the calculation are described by Bernard et al. (4).

Finally, we calculated the physical center of the embolism-affected pieces as well as of the whole lung. The center is simply the mean *x*, *y*, and *z* coordinates of the pieces considered. We tested the hypothesis that the embolism pieces are centered at the same coordinates as all the pieces by using a paired *t*-test on each dimension (*x*, *y*, and *z*). The shift from the center of the whole lung to the center of the embolism is a descriptive statistic that can help in visualizing the relative position of the embolized regions.

RESULTS

All animals had a normal hemodynamic profile at the beginning of the study, as shown in Table 1. The decrease in heart rate, increases in systemic and pulmonary arterial pressures, and decreases in arterial oxygenation seen in this study are consistent with the results of other studies reporting the effects of venous air embolism (2, 5, 9, 13, 27, 46). Cardiac output did not change significantly during the study period.

The primary focus of this study was to examine the spatial distribution of 15-μm fluorescent microspheres before, during, and after the venous embolization of N_2 bubbles. Because fluorescent microspheres are a reliable indicator of regional PBF (16), we assumed that regions with a substantial decrease in PBF after the

Table 1. *Hemodynamic parameters*

	AWP, cmH_2O	MAP, mmHg	MPP, cmH_2O	HR, beats/min	CO, l/min	Pa_{O_2}, Torr	Pa_{CO_2}, Torr
B	9.8 ± 0.5	103 ± 11	12.6 ± 1.3	141 ± 6	4.30 ± 0.20	97.8 ± 2.0	38.8 ± 1.1
$N_2$15	11.5 ± 0.5	127 ± 9	35.5 ± 4.9	139 ± 14	4.59 ± 0.44	47.8 ± 3.9	50.3 ± 1.4
$N_2$30	11.5 ± 0.6	124 ± 10	34.2 ± 4.6	95 ± 12	4.59 ± 0.72	38.6 ± 4.9	57.5 ± 1.9
R15	11.2 ± 0.8	105 ± 11	23.2 ± 4.0	145 ± 13	4.05 ± 0.52	61.6 ± 7.3	53.9 ± 2.5
R30	11.0 ± 0.7	106 ± 4	18.2 ± 5.1	144 ± 4	3.96 ± 0.30	70.5 ± 8.2	49.8 ± 4.5
			P values				
$N_2$15 vs. B	0.0005	0.05	0.003	0.9	0.4	<0.0001	0.0002
$N_2$30 vs. $N_2$15	1.0	0.2	0.003	0.04	0.7	<0.0001	0.0001
$N_2$30 vs. B	0.0005	0.7	0.5	0.03	1.0	0.005	0.004
R15 vs. $N_2$30	0.5	0.1	0.04	0.03	0.2	0.01	0.2
R30 vs. R15	0.4	0.9	0.1	1.0	0.9	0.004	0.2
R30 vs. B	0.06	0.8	0.3	0.6	0.4	0.03	0.07

Hemodynamic parameters are means ± SE of 6 dogs for each study condition. B, baseline; $N_2$15 and $N_2$30, 15 and 30 min of N_2 embolism; R15 and R30, 15 and 30 min of recovery; AWP, peak airway pressure; MAP, mean systemic arterial pressure; MPP, mean pulmonary arterial pressure; HR, heart rate; CO, cardiac output; Pa_{O_2} and Pa_{CO_2}, arterial P_{O_2} and P_{CO_2}. $P < 0.05$ (by paired *t*-test) is considered statistically significant.

infusion of N_2 would be indicative of the presence of emboli.

Analysis of Slopes in Each Spatial Dimension

The WNRF for each lung piece analyzed was plotted against each of the four spatial dimensions studied (*x*, *y*, *z*, and *h*), and slopes were determined as described in MATERIALS AND METHODS. Figure 1 shows an example of the baseline WNRF values plotted against the dorsal-to-ventral (*y*) dimension, and Fig. 2 shows the same animal and spatial dimension at $N_2$15. Figure 3 shows the change in slope between these two conditions as a result of subtraction and illustrates that, in almost every lung piece in the ventral aspect of the animal, there was a substantial flow decrease, whereas in the dorsal lung regions there were areas of dramatic increases and decreases in flow. Results of least squares regression of these plots show no statistically significant changes in the slopes of the blood flow distribution in the *x* and *z* distributions, but the changes in the *y* and *h* slopes were statistically significant. For each dimension the slopes for $N_2$30-$N_2$15 are quite small and nonsignificant, indicating that the embolism process had reached a relatively steady state by 15 min. The results of the least squares regressions in each spatial dimension are shown in Table 2. All subsequent analyses of changes in PBF distribution were performed only in the *y* and *h* distributions.

Regression Analysis in the Vertical and Hilar-to-Peripheral Dimensions

Data were analyzed for all animals to determine the incidence of embolism at $N_2$15 and $N_2$30 in the *y* and *h* dimensions for each animal. Embolism affected a large fraction of the lung. Among the six animals, 48–71% of pieces lost ≥10% of their relative flow ($N_2$15 compared with baseline) with a mean of 62% of pieces. The results were plotted as illustrated in Figs. 4 and 5, which indicate strong trends in the incidence of embolism across the *y* and *h* dimensions. In addition, the fraction of pieces with a >10% decrease in WNRF at $N_2$15 and $N_2$30 was plotted against the initial WNRF at baseline conditions, as illustrated in Fig. 6. The purpose was to determine whether there was any tendency for N_2

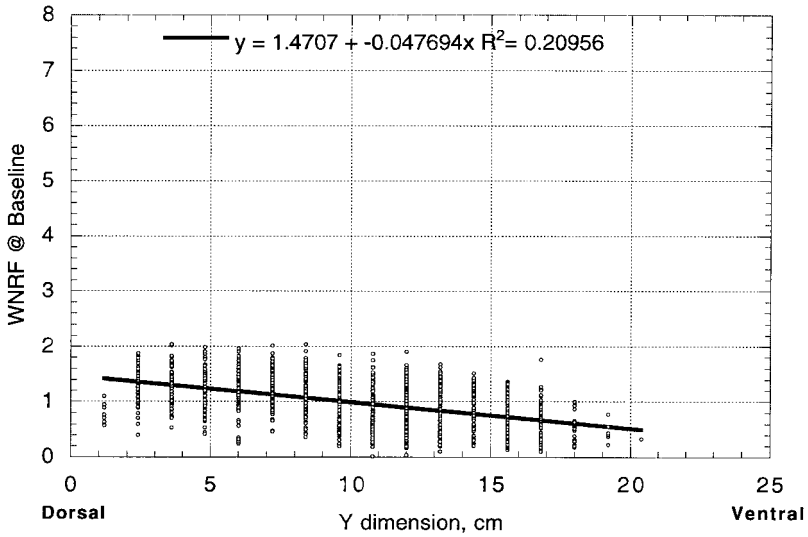

Fig. 1. Weight-normalized relative pulmonary blood flow (WNRF) in vertical (*y*) dimension at baseline conditions in a representative animal (*dog 3*). WNRF decreases in dorsal-to-ventral direction with animal in supine position.

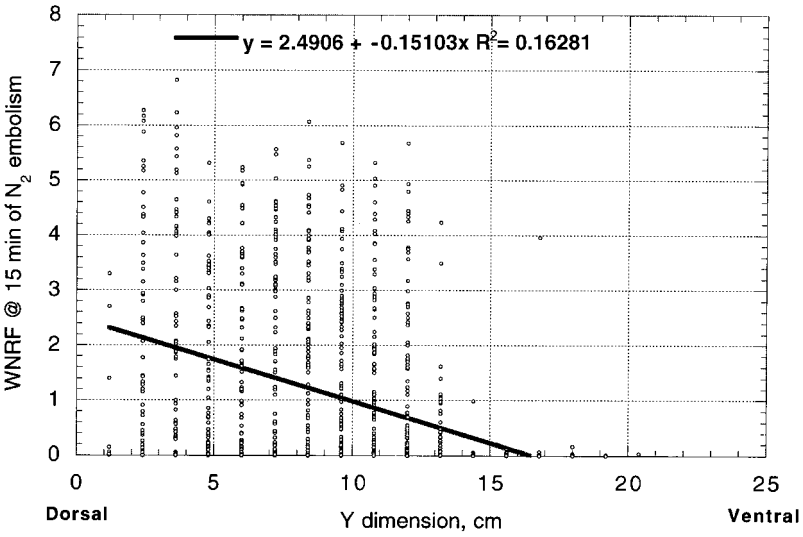

Fig. 2. WNRF in *y* dimension in *dog 3* after 15 min of administration of a venous N_2 infusion. Flow is almost absent in ventral portions of lung, and range of pulmonary blood flow is much wider in perfused lung regions than in Fig. 1.

emboli to go to lung areas with a particular baseline flow (i.e., whether high-flow pieces demonstrate a greater incidence of embolism than low-flow pieces). No striking trend of embolism incidence with baseline flow is evident from Fig. 6, but, as noted below, a small but statistically significant trend does exist after controlling for confounding from the effects of *y* and *h*.

Univariate and multivariate regression analyses were performed for the influence of *y*, *h*, and baseline on the dichotomous indicator of embolism. All animals were studied at $N_2$15 and $N_2$30, and the mean results across the six animals are summarized in Table 3. On the basis of the results of the regression analysis, we can confirm the previous findings of Chang et al. (10, 11) that in the supine position the emboli clearly distribute in a manner consistent with their buoyancy. The influence of *y* is by far the strongest of the three factors, as indicated by R^2 or ΔR^2 for the $N_2$15 or $N_2$30 embolism incidence: R^2 is 24–25% for *y*, 6–7% for *h*, and 2–3% for baseline. Values for ΔR^2 are somewhat smaller but show the same dominance for *y*, followed by *h*, then baseline. The slope of embolism incidence is also stronger for *y* (mean slope = 6%) than for *h* (3–4% across types of analyses and times). In stepwise regression analyses of embolism incidence, factors were selected into the regression model in the order *y*, *h*, and baseline for every animal. Table 3 also shows only small and nonsignificant changes in slopes between $N_2$15 and $N_2$30. The *h* distribution of the emboli documented in Table 3 has not been previously shown. The reversal of sign of the mean slope for baseline from univariate to multivariate analysis is notable and arises from the positive correlation and trend of baseline flow with the vertical and radial dimensions. Thus, in analyzing the influence of baseline flow on embolism, it is essential to control for *y* and *h*.

Regression Analysis Performed Against Baseline WNRF

To analyze whether more emboli distribute to areas where there is more flow while controlling for the strong influences of the *y* and *h* dimensions, we performed a second set of regression analyses. As a very

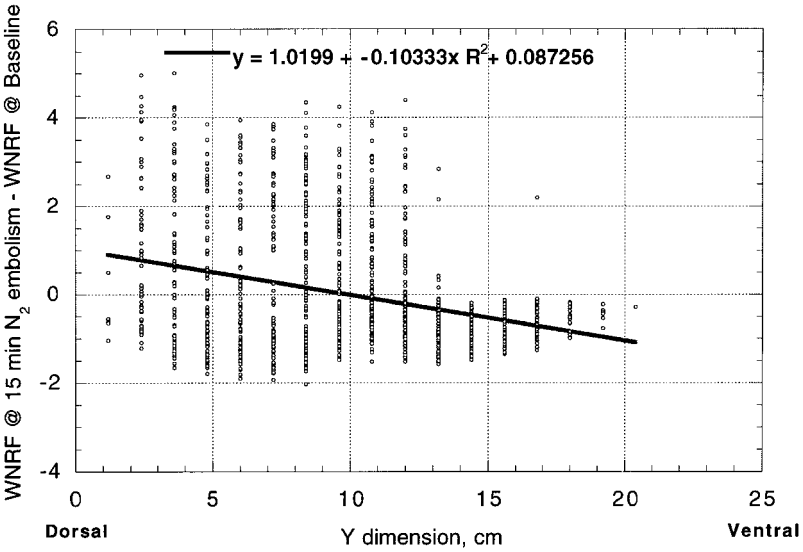

Fig. 3. Comparison of changes in slopes between 15 min of N_2 embolism and baseline condition in *dog 3* (see Figs. 1 and 2) performed by subtraction. Values below zero on *y*-axis indicate lung regions in which flow was decreased; values above zero are lung regions in which flow was increased.

Table 2. *Mean slope values*

Slope Comparisons	Dimension			
	x	*y*	*z*	*h*
$N_2$15-B	−1.2 ± 2.6 (*P* = 0.7)	−13.4 ± 1.8 (*P* = 0.0007)	0.2 ± 0.8 (*P* = 0.8)	−9.1 ± 1.6 (*P* = 0.002)
$N_2$30-B	−1.5 ± 2.9 (*P* = 0.6)	−12.4 ± 1.9 (*P* = 0.001)	−1.0 ± 0.5 (*P* = 0.1)	−7.6 ± 1.0 (*P* = 0.0006)
$N_2$30-$N_2$15	−0.1 ± 1.1 (*P* = 0.9)	1.1 ± 1.0 (*P* = 0.3)	−1.2 ± 0.5 (*P* = 0.07)	1.5 ± 1.6 (*P* = 0.4)

Values are means ± SE of 6 animals expressed as %/cm. Slope comparison reflects later condition vs. earlier condition. *x*, Lateral; *y*, vertical; *z*, horizontal; *h*, radial. Slopes were generated for each condition by method of least squares, and comparisons were made by subtraction of slopes for 2 conditions. A single-sample *t*-test was used to determine whether changes were statistically significant.

strong control for the linear influence of *y* and *h*, we first regressed the dichotomous embolism indicator on *y* and *h* and then regressed the residuals from this first step on baseline. (The methodology is analogous to partial correlation.) The coefficient of baseline in the second regression analysis is, then, a conservative estimate of the trend in embolism incidence with baseline flow. The regression analysis was carried out for the embolism indicator at $N_2$15 and, separately, for $N_2$30. The same regression analyses based on residuals were also carried out using the actual flow change for each piece at $N_2$15 (i.e., flow at $N_2$15 minus flow at baseline). The null hypothesis of no effect of baseline flow was tested using the two-sided single-sample *t*-test comparing each mean regression coefficient with zero. The results of the regression analyses performed for incidence of embolism and change in flow vs. baseline are summarized in Table 4. The trend in incidence of embolism with baseline flow is positive and statistically significant at $N_2$15 (P = 0.01), and the decrease in actual flow vs. baseline is also statistically significant (P = 0.005). The trend in embolism with baseline at $N_2$30 is also positive but not significant. R^2 is very small for all these analyses.

Because a statistical phenomenon called "regression to the mean" can induce a significant negative association when a change is compared with the starting

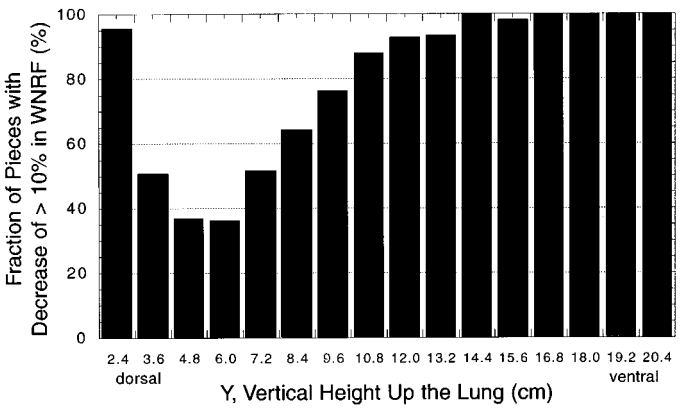

Fig. 4. Percentage of lung pieces that demonstrated a >10% decrease in pulmonary blood flow in each vertical plane that was generated during data processing in a representative animal (*dog 2*) after 15 min of N_2 embolism.

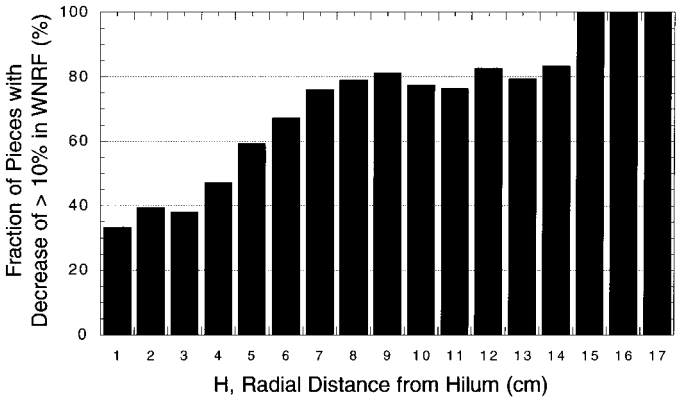

Fig. 5. Percentage of lung pieces that demonstrated a >10% decrease in pulmonary blood flow in hilar-to-peripheral (*h*) dimension in *dog 2* after 15 min of N_2 embolism.

value, we carried out an analysis of actual flow change from baseline to R30, a flow change with a relationship to baseline flow that would be primarily due to regression to the mean. Regression analyses were performed on the actual flow changes (i.e., R30 − baseline) vs. baseline flow, as described above, and the results again were compared with zero by using the two-sided single-sample *t*-test. These results are also displayed in Table 4. The "baseline effect" is observed much less at R30 (slope = −5.4%) than at $N_2$15 (slope = −35.8%). Therefore, the tendency of emboli to distribute to lung regions with higher flow is not the result of regression to the mean. On the basis of these results, we can conclude that there is a weak but significant tendency for the emboli to distribute to lung regions that have a higher PBF.

Center of Embolism and Center of Lung Studies

We calculated the center of the embolism by calculating the mean *x*, *y*, and *z* coordinates for all the pieces with a positive embolism indicator. Next, we calculated the center of the lung by determining the mean *x*, *y*, and *z* coordinates for each animal. These two centers were then compared using a single-sample *t*-test (2-tailed). The embolism pieces (those with the positive embolism

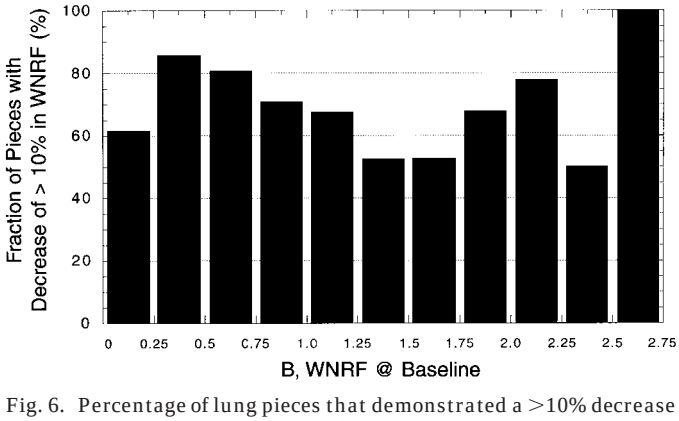

Fig. 6. Percentage of lung pieces that demonstrated a >10% decrease in pulmonary flood flow in *dog 2* after 15 min of N_2 embolism plotted as a function of their initial flow values at baseline (B) conditions. Emboli appear to distribute to lung regions that have initially low- and high-flow pieces.

Table 3. *Regression models for incidence of embolism as a function of spatial dimension or baseline flow*

Type of Analysis	Embolism Incidence								Change in Incidence $N_2$30-$N_2$15	
	$N_2$15				$N_2$30					
	Slope, %	*P* (vs. 0)	R^2, %	ΔR^2, %	Slope, %	*P* (vs. 0)	R^2, %	ΔR^2, %	Slope diff, %	*P* ($N_2$30-$N_2$15)
					y Dimension					
Univariate	5.8 ± 0.6	0.0003	24.0 ± 4.9		6.0 ± 0.8	0.0007	25.0 ± 5.7		0.2 ± 0.2	0.5
Multivariate	5.8 ± 0.6	0.0003		24.0 ± 4.9	5.8 ± 0.8	0.001		25.0 ± 5.7	0.0 ± 0.3	0.9
					h Dimension					
Univariate	3.8 ± 0.7	0.003	5.8 ± 1.6		4.2 ± 0.7	0.002	6.6 ± 1.9		0.5 ± 0.5	0.4
Multivariate	3.2 ± 0.5	0.002		3.4 ± 1.4	3.6 ± 0.3	<0.0001		3.7 ± 0.8	0.3 ± 0.5	0.5
					Baseline flow					
Univariate	−12.5 ± 5.3	0.06	2.3 ± 0.8		−15.0 ± 5.9	0.052	2.9 ± 1.0		−2.5 ± 1.6	0.2
Multivariate	9.0 ± 2.1	0.008		0.6 ± 0.2	6.4 ± 3.4	0.1		0.6 ± 0.2	−2.5 ± 1.9	0.2

Values are means ± SE of univariate and multivariate regression analyses in vertical (*y*) and hilar-to-peripheral (*h*) dimensions compared with baseline; results of initial univariate and multivariate regression analyses against initial baseline flow values are also presented. Univariate regression includes only specified dimension or baseline flow as an independent variable. Multivariate regression includes *y* and *h* dimensions and baseline flow; mean slope is from multivariate model, and ΔR^2 is increase in R^2 when *y* or *h* dimension or baseline flow is added to a model including only the other 2 independent variables.

indicator) are centered at a small but statistically significant distance from the center of the lung. The shift is 1.5 ± 0.3 (SE) cm in the vertical direction (P = 0.004 compared with zero shift) and 0.4 ± 0.1 cm (P = 0.004) radially from the hilum. The total span of the vertical and radial dimensions of the lung is ~20 cm, making the vertical and radial embolism shifts ~8 and 2% of each dimension, respectively. Mean shifts in the other dimensions were minor: 0.1 ± 0.3 and 0.2 ± 0.3 cm for *x* and *z*, respectively.

Variance Components Study

Embolism induced enormous changes in flow distribution, as indicated by the variance components analysis: 57 ± 1 (SE) % of the overall variation in flow (across pieces and conditions) was due to embolism, time, and methodological noise. Conversely, 43% of flow variation was due to biological structure or the piece effect in the pattern of flow distribution common to both states. For minor interventions such as exercise, the piece effect is generally 70–80% [e.g., 80% for exercising horses (4)]. For no intervention but the passage of time, the combination of time and methodological noise usually contributes ≤10% (17) to the total piece effect.

Table 4. *Association of baseline flow with embolism and recovery*

Response Variable	Regression Coeff for Baseline Flow, %	*P**	R^2, %
Incidence of embolism			
$N_2$15	6.4 ± 1.7	0.01	0.6 ± 0.3
$N_2$30 vs. B	4.6 ± 2.5	0.5	0.6 ± 0.3
Actual flow change			
$N_2$15 vs. B	−35.8 ± 7.3	0.005	0.5 ± 1.9
R30 vs. B	−5.4 ± 3.7	0.2	2.9 ± 1.5

Values are means ± SE of additional regression analyses performed to determine whether N_2 emboli preferentially distribute to areas with initially higher levels of flow; n = 6. This second set of regression analysis controls for strong influences of *y* and *h* dimensions. Each response variable is residual after multivariate regression on *y* and *h* dimensions. *Null hypothesis: mean value of coefficient = 0 (*t*-test).

DISCUSSION

Methodological Issues

Microspheres have been used to measure regional organ perfusion for many years, and this method has generally been accepted as reliable and well validated (24). However, because microspheres are particulates, it is possible that they may not behave comparably to blood when one is attempting to measure flow distributions at the level of capillaries (51). This issue was addressed by Bassingthwaigthe et al. (3) in their validation of microspheres for measurement of regional myocardial blood flow values. Regional organ perfusion as measured using a molecular tracer of blood flow (1-iododesmethylimipramine) was highly correlated with flow measured by radiolabeled microspheres. These investigators concluded that microspheres accurately measure regional blood flow, even when the region in question is supplied by an artery with a diameter only a few times larger than the 15-μm diameter of the microsphere. Because the regions of lung that were studied in this investigation are supplied by arterioles that average 50–100 μm in diameter, the use of 15-μm microspheres to measure regional organ perfusion should result in an accurate assessment of the true regional PBF.

This investigation used fluorescent microspheres, rather than radiolabeled microspheres, to measure regional organ perfusion. To reliably measure regional PBF, the 15-μm fluorescent microspheres used in this study must have a distribution in the microcirculation that is similar to the distribution of blood and must be highly correlated with the measurements obtained using radiolabeled microspheres. Because the 15-μm fluorescent microspheres have a density very close to that of blood (1.02 g/ml), their distribution in the

circulation should be similar to that of blood; indeed, this validation in dogs has been published (16). In addition, the number of microspheres in each lung piece must be great enough to limit the effect of method error on the statistical analysis. With an injection of $2–3 \times 10^6$ microspheres per condition, each tissue piece would have >350 microspheres, even when PBF to that piece was decreased by 75%. Because the entire lung was analyzed and, therefore, contained some subpleural pieces that might be smaller than the majority of pieces, the samples were normalized by weight to correct for differences in parenchymal volume. In addition, samples containing >25% airway tissue or samples that were noticeably abnormal (i.e., contained clot or had compacted tissue) were excluded from the statistical analysis.

In this particular experiment a potential problem with ensuring adequate numbers of microspheres per piece of lung tissue is that of occluding too many pulmonary vessels by using the microsphere technique. This would not normally be of concern if emboli were not present. However, it is likely that there are adequate numbers of patent pulmonary capillaries, even in the presence of the N_2 emboli. Microspheres tend to lodge primarily in capillaries or in the terminal arteriole just before its branching into capillaries and can move slowly along the length of a capillary, eventually lodging in a <15-μm-diameter vessel (up to 20% smaller) (23). A recent study (15) in dog lungs gave a terminal arteriolar diameter of 28 μm, which is substantially larger than the size of a microsphere and implies that microspheres would lodge in capillaries. In another study (31) the authors summarize many of the known studies of vascular morphometry and make model predictions which indicate that there should be $\sim 1 \times 10^9$ vessels of 10–15 μm in diameter. The total number of microspheres injected per dog was 1.1×10^7 (only one of the five injections required 3×10^6 microspheres), which would occlude ~1% of these vessels. Because it is possible that 15-μm microspheres could lodge in series in a given vessel (40), then even <1% of the vessels might be occluded by microspheres. N_2 emboli were presumed to be present in a lung piece when there was a >10% (of baseline) decrease in relative PBF. A mean of ~60% of the lung pieces studied had a positive embolism indicator. This does not necessarily mean that 60% of the 15-μm vessels were occluded. Rather, it is more likely that 10% of the vessels in the affected 60% of the lung (or a total of ≥6% of the lung) have been embolized. Therefore, one could conclude that, between microspheres and N_2 emboli, ~90% of the lung capillaries remained patent during the study.

The lungs were dried at TLC, meaning that alveolar volumes will be uniformly distended throughout the lung while it is drying. This may not be true of the lung at TLC in the intact animal. The configuration of the lung after drying may be different from that of the lung in vivo for other reasons as well. First, lung drying is performed with a constant pressure of ~35 cmH_2O while the lung is suspended from the trachea, so that lung volumes (and, consequently, the linear dimensions of the 3 axes) are increased compared with the in vivo lung. In addition, the influence of gravity in a lung suspended from the trachea will differ from that in a supine animal, possibly resulting in a slight distortion of the lung configuration compared with the in vivo condition. Another difference is the lack of physical constraint imposed by the chest wall and diaphragm in the intact animal and the compression of the lung regions that lie below the heart when the animal is supine. It is anticipated that these conditions might impose a different shape on the intact lung. These factors are difficult to quantitate or evaluate, much less to correct for. However, because the effect of N_2 embolism is so profound and results in such an extreme series of changes in the distribution of PBF, we expect the conformational differences between the air-dried and the in vivo lung to be unimportant with respect to the results of this study. In addition, because the fluorescent microspheres should remain fixed in the vessels after lodging in vivo, the relative perfusion changes to the different lung regions should remain fixed as well.

Vertical Distribution

Under baseline conditions, we clearly observed a predominance of PBF to the dorsal lung regions in the supine dog. This has been observed previously, and this dorsal flow predominance persists in animals in the prone position (17, 33, 49, 50). This finding suggests that gravity does not play a dominant role in determining the heterogeneity of PBF in quadrupeds when perturbations other than anesthesia, intubation, and mechanical ventilation are absent (4, 25). With N_2 embolism, the distribution of PBF in the *y* gradient showed a strong tendency for the bubbles to distribute according to their buoyancy, i.e., a gravitational dependence such that the bubbles "float to the top." This strong *y* gradient was most evident in the results of the center-of-embolism study performed on our data. Because the total span of the *y* distance was ~20 cm, the center of embolism shifted from the center of the lung vertically by ~8% of this distance. This confirms the original findings in the supine dog and the model predictions made by Chang et al. (10, 11). However, our study is still limited, because it does not give any indication of the size or shape of the region(s) most impacted by the embolism.

The *y* distribution of the emboli at $N_2$30 is not significantly different from that at $N_2$15, as shown in Table 3. This is probably because the process of embolization has reached a steady state by 15 min. The way in which such a steady state could result can be hypothesized as follows: vessels at the top of the lung are blocked by the bubbles that arrive when embolism initially starts, and therefore the subsequent incoming bubbles must distribute to the lower, dependent lung regions. As the lodged bubbles resolve with time, emboli could once again distribute to the nondependent portions of the lung. With continuous bubble administration balanced by continuous bubble resorption, it is possible that the distribution of emboli in the lung

could become uniform, if it is assumed that the dog could survive a certain level of embolization for a long enough period of time (45). There is some evidence that this was beginning to occur by $N_2$30, as evidenced in Table 1. When the values for $N_2$15 and $N_2$30 are compared with the baseline values, the *P* values for the mean systemic arterial pressure and mean pulmonary arterial pressure are not significantly different at $N_2$30, but they are at $N_2$15. Also, the *P* values are smaller for the arterial P_{O_2} and P_{CO_2}, although they are still significantly different from the baseline. Because this study used a decrease of regional flow as an indicator of the presence of an embolism, we also cannot say whether another embolism could lodge more proximally in the same blood vessel as a result of reestablishment of flow or even in the continued presence of an occlusion to flow, as has been seen previously (40).

Hilar-to-Peripheral Distribution

Evidence for an *h* distribution of gaseous emboli has not been previously presented, nor has it been theoretically postulated. However, it is logical to assume that such a distribution would occur with gaseous emboli, because the emboli would travel along the pulmonary arteries until they reached a vessel that was too small to permit further passage. However, when a bubble reaches a bifurcation in the vessel, the next determinant of the path of the bubble could be flow or buoyancy, as illustrated in Fig. 7. In this study we found that both factors influence the behavior of the bubble, and therefore both should exert an influence on bubble distribution at such a bifurcation. The relative contribution of each factor at such a vascular bifurcation remains to be determined.

The *h* gradients for PBF have been demonstrated for dogs (17, 19, 20, 22), humans (21), sheep (50), and ponies (30). Walther et al. (50), using methods similar to those for this study, concluded that the normal *h* distribution of PBF was likely a function of vascular anatomy due to branching vascular patterns and regional variations in capillary density. If the *h* blood flow gradient is reflective of the inherent structure of the pulmonary vessels, then an *h* distribution of gaseous emboli as seen in this study may also reflect the influence of vascular structure on bubble distribution. However, because the variance-components study that we performed indicates that, on average, only 43–44% of the flow variation could be explained by the configuration of the biological structure, then one might conclude that vascular structure does not play the most important role in determining the distribution of gaseous emboli.

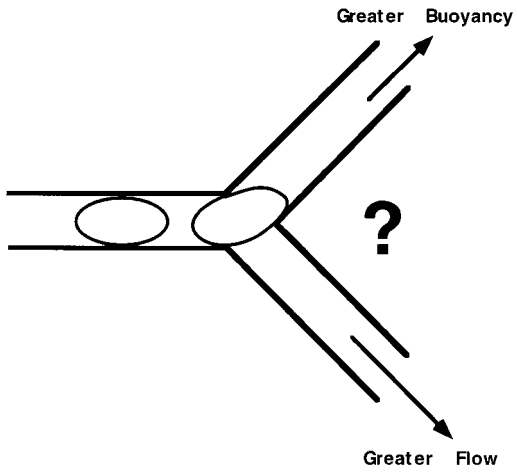

Fig. 7. Graphic illustration of a gas bubble reaching a bifurcation in pulmonary vascular tree. It appears that buoyancy and flow control movement of bubble; although effect of buoyancy appears to be quite a bit stronger.

Distribution According to Baseline Flow

The preferential distribution of N_2 emboli to lung regions of initially higher flow is a new finding that reflects an advantage of the methodology used and the superior level of resolution that it affords. Although the influence of baseline flow on the distribution of gaseous pulmonary emboli is small, it is nevertheless statistically significant and evidently real. As shown in Table 1, there are no statistically significant changes in cardiac output between baseline and the two embolism conditions. Because previous studies of N_2 embolism have shown that it does not produce an increase in shunt (27), then the total amount of blood flowing through the pulmonary circulation per minute should be approximately the same in each of these three conditions. Therefore, redistribution of PBF from lung regions of initially higher blood flow to lung regions of initially lower blood flow could be accounted for partly by the effects of the embolism.

In addition, the distribution of emboli according to flow is most evident when the baseline flow is compared with the flow at $N_2$15, rather than at $N_2$30. This is because at $N_2$30, there are already bubbles present and severe aberrations of PBF have already resulted. Therefore, at $N_2$30 the bubbles are now distributing according to the flow patterns observed at $N_2$15, and not at baseline. This is why the flow effect is seen less prominently at $N_2$30.

Although the flow effect is small, it is most likely real and not the result of regression to the mean. This is evidenced by the fact that the baseline slope from the regression analysis at R30 is much smaller than the baseline slope at $N_2$15. Regression to the mean would tend to affect both slopes.

Embolism Methodology

Bubble size was estimated using a method that is not highly accurate; however, the measured size at the time and site of infusion will likely be quite different from the size that is embolized into the pulmonary vasculature. This is due to the passage of the bubbles through the right side of the heart, which mixes the bubbles in the blood and would likely result in a change in size of the infused bubbles. Although this may not represent the fate of bubbles in the venous circulation during decompression, it is a realistic reproduction of accidental venous air embolism in clinical scenarios. However,

not many studies address the changes in size of bubbles, and those that do have studied the effects of different gas types on the size of the bubbles (8, 37, 39, 41). A recent modeling study (42) of stabilized bubbles in the circulation indicates that bubbles reach maximal size in the pulmonary small vessel beds because blood pressure is low, there is no inherent unsaturation, and gases from the alveoli diffuse into the bubble. Therefore, even very small bubbles that might have traversed other capillary beds will ultimately become lodged in the pulmonary bed. This might explain why it has been observed that the lung is such a highly effective filter of bubbles (6, 46). For gaseous emboli, it is likely that surface-active molecules in blood could aggregate at bubble surfaces and provide a stabilizing action, but there is no experimental evidence for this.

Another consideration when studying distributions of gaseous emboli in the lungs is the reaction by the lung vasculature caused by the lodging of such emboli. Gaseous emboli cause microvascular injury and the release of inflammatory mediators by the lung (14, 34), which may then have systemic circulatory effects (28). We saw no changes in cardiac output resulting from these physiological effects. However, there are profound alterations in systemic and pulmonary arterial pressures, which may exert a different influence on the distributions of emboli that enter the lungs later, after embolism has been occurring for a while. We did not attempt to correlate the levels of circulating inflammatory mediators with the changes in regional distribution of PBF, although this might be an important endeavor for the future. We also did not attempt to inhibit the release of such inflammatory mediators to attempt to study a "pure buoyancy" effect. In this investigation our goal was to study the animal in as much of an intact and unaltered state as possible, mimicking actual accidental N_2 embolism.

Conclusion

The results of this study demonstrate that the use of higher resolution methods to determine the distribution of PBF provides new information about such distributions. In addition to the influence of buoyancy, the distribution of gaseous emboli is influenced by regional lung blood flow. We also observed an *h* distribution of gaseous emboli, which has not been described previously and may be reflective of inherent lung vascular structure. Therefore, we conclude that the distribution of gaseous emboli in the pulmonary blood vessels is influenced not only by their differential density from blood but also by the flow dynamics within the pulmonary vascular tree.

We acknowledge the excellent technical assistance of Erin Shade, Dowon An, and Emily Anderson. We gratefully acknowledge the input of Robb W. Glenny regarding the many facets of the fluorescent microspheres technique.

Support for this project was provided in part by National Heart, Lung, and Blood Institute Grants HL-12174 and HL-24163.

Address for reprint requests and other correspondence: J. E. Souders, Pulmonary and Critical Care Medicine, Box 356522, University of Washington, Seattle, WA 98195-6522 (E-mail: jsouders@u.washington.edu).

Received 28 December 1998; accepted in final form 13 July 1999.

REFERENCES

1. **Albertine, K. H., J. P. Wiener-Kronish, K. Koike, and N. C. Staub.** Quantification of damage by air emboli to lung microvessels in anesthetized sheep. *J. Appl. Physiol.* 57: 1360–1368, 1984.
2. **Atkins, C. E., C. E. Lehner, K. A. Beck, R. R. Dubielzig, E. V. Nordheim, and E. H. Lanphier.** Experimental respiratory decompression sickness in sheep. *J. Appl. Physiol.* 65: 1163–1171, 1988.
3. **Bassingthwaighte, J. B., M. A. Malone, T. C. Moffett, R. B. King, S. E. Little, J. M. Link, and K. A. Krohn.** Validity of microsphere deposition for regional myocardial flows. *Am. J. Physiol.* 253 (*Heart Circ. Physiol.* 22): H184–H193, 1987.
4. **Bernard, S. L., R. W. Glenny, H. H. Erickson, M. R. Fedde, N. L. Polissar, R. J. Basaraba, and M. P. Hlastala.** Minimal redistribution of pulmonary blood flow with exercise in racehorses. *J. Appl. Physiol.* 81: 1062–1070, 1996.
5. **Butler, B. D., J. Conkin, and S. Luehr.** Pulmonary hemodynamics, extravascular lung water and residual gas bubbles following low dose venous gas embolism in dogs. *Aviat. Space Environ. Med.* 60: 1178–1182, 1989.
6. **Butler, B. D., and B. A. Hills.** The lung as a filter for microbubbles. *J. Appl. Physiol.* 47: 537–543, 1979.
7. **Butler, B. D., and B. A. Hills.** Transpulmonary passage of venous air emboli. *J. Appl. Physiol.* 59: 543–547, 1985.
8. **Butler, B. D., B. C. Leiman, and J. Katz.** Arterial air embolism of venous origin in dogs: effect of nitrous oxide in combination with halothane and pentobarbitone. *Can. J. Anaesth.* 34: 570–575, 1987.
9. **Butler, B. D., R. Robinson, T. Little, J. E. Chelly, and M. F. Doursout.** Cardiopulmonary changes with moderate decompression in rats. *Undersea Hyperb. Med.* 23: 83–89, 1996.
10. **Chang, H. K., L. Delaunois, R. Boileau, and R. R. Martin.** Redistribution of pulmonary blood flow during experimental air embolism. *J. Appl. Physiol.* 51: 211–217, 1981.
11. **Chang, H. K., M. E. Weber, J. Thomson, and R. R. Martin.** Hydrodynamic features of pulmonary air embolism: a model study. *J. Appl. Physiol.* 51: 1002–1008, 1981.
12. **Cockett, A. T., S. M. Pauley, D. N. Zehl, A. A. Pilmanis, and W. S. Cockett.** Pathophysiology of bends and decompression sickness. An overview with emphasis on treatment. *Arch. Surg.* 114: 296–301, 1979.
13. **Deal, C. W., P. Barton, F. Fielden, and I. Monk.** Hemodynamic effects of pulmonary air embolism. *J. Surg. Res.* 11: 533–538, 1971.
14. **Flick, M. R., J. M. Hoeffel, and N. C. Staub.** Superoxide dismutase with heparin prevents increased lung vascular permeability during air emboli in sheep. *J. Appl. Physiol.* 55: 1284–1291, 1983.
15. **Gan, R. Z., and R. T. Yen.** Vascular impedance analysis in dog lung with detailed morphometric and elasticity data. *J. Appl. Physiol.* 77: 706–717, 1994.
16. **Glenny, R. W., S. Bernard, and M. Brinkley.** Validation of fluorescent-labeled microspheres for measurement of regional organ perfusion. *J. Appl. Physiol.* 74: 2585–2597, 1993.
17. **Glenny, R. W., W. J. E. Lamm, R. K. Albert, and H. T. Robertson.** Gravity is a minor determinant of pulmonary blood flow distribution. *J. Appl. Physiol.* 71: 620–629, 1991.
18. **Glenny, R. W., N. L. Polissar, S. McKinney, and H. T. Robertson.** Temporal heterogeneity of regional pulmonary perfusion is spatially clustered. *J. Appl. Physiol.* 79: 986–1001, 1995.
19. **Hakim, T. S., G. W. Dean, and R. Lisbona.** Effect of body posture on spatial distribution of pulmonary blood flow. *J. Appl. Physiol.* 64: 1160–1170, 1988.
20. **Hakim, T. S., G. W. Dean, and R. Lisbona.** Quantification of spatial blood flow distribution in isolated canine lung. *Invest. Radiol.* 23: 498–504, 1988.
21. **Hakim, T. S., R. Lisbona, and G. W. Dean.** Gravity-independent inequality in pulmonary blood flow in humans. *J. Appl. Physiol.* 63: 1114–1121, 1987.

22. **Hakim, T. S., R. Lisbona, and G. W. Dean.** Effect of cardiac output on gravity-dependent and nondependent inequality in pulmonary blood flow. *J. Appl. Physiol*. 66: 1570–1578, 1989.
23. **Hales, J. R. S., and W. J. Cliff.** Direct observations of the behaviour of microspheres in microvasculature. *Bibl. Anat*. 15: 87–91, 1977.
24. **Heyman, M. A., B. D. Payne, J. I. Hoffman, and A. M. Rudolf.** Blood flow measurement with radionuclide-labeled particles. *Prog. Cardiovasc. Dis*. 20: 55–79, 1977.
25. **Hlastala, M. P., S. L. Bernard, H. H. Erickson, M. R. Fedde, E. M. Gaughan, R. McMurphy, M. J. Emery, N. L. Polissar, and R. W. Glenny.** Pulmonary blood flow distribution in standing horses is not dominated by gravity. *J. Appl. Physiol*. 81: 1051–1061, 1996.
26. **Hlastala, M. P., M. A. Chornuk, D. A. Self, H. J. Kallas, J. W. Burns, S. Bernard, N. L. Polissar, and R. W. Glenny.** Pulmonary blood flow redistribution by increased gravitational force. *J. Appl. Physiol*. 84: 1278–1288, 1998.
27. **Hlastala, M. P., H. T. Robertson, and B. K. Ross.** Gas exchange abnormalities produced by venous gas emboli. *Respir. Physiol*. 36: 1–17, 1979.
28. **Huang, K. L., and Y. C. Lin.** Activation of complement and neutrophils increases vascular permeability during air embolism. *Aviat. Space Environ. Med*. 68: 300–305, 1997.
29. **James, P. B.** Dysbarism: the medical problems from high and low atmospheric pressure. *J. R. Coll. Physicians Lond*. 27: 367–374, 1993.
30. **Jarvis, K. A., E. P. Steffey, W. S. Tyler, N. Willits, and M. Woliner.** Pulmonary blood flow distribution in anesthetized ponies. *J. Appl. Physiol*. 72: 1173–1178, 1992.
31. **Krenz, G. S., J. H. Linehan, and C. A. Dawson.** A fractal continuum model of the pulmonary arterial tree. *J. Appl. Physiol*. 72: 2225–2237, 1992.
32. **Loewenherz, J. W.** Pathophysiology and treatment of decompression sickness and gas embolism. *J. Fla. Med. Assoc*. 79: 620–624, 1992.
33. **Mure, M., K. B. Domino, H. T. Robertson, M. P. Hlastala, and R. W. Glenny.** Pulmonary blood flow does not redistribute in dogs with reposition from supine to left lateral position. *Anesthesiology* 89: 483–492, 1998.
34. **Ohkuda, K., K. Nakahara, A. Binder, and N. C. Staub.** Venous air emboli in sheep: reversible increase in lung microvascular permeability. *J. Appl. Physiol*. 51: 887–894, 1981.
35. **Oyama, Y., and M. P. Spencer.** Cardiopulmonary effects of intravenous gas embolism; with special reference to fate of intravascular gas bubbles. *Jpn. Circ. J*. 35: 1541–1549, 1971.
36. **Pilmanis, A. A.** (Editor). *Proceedings of the 1990 Hypobaric Decompression Sickness Workshop*. Brooks AFB, TX: US Air Force Armstrong Laboratory, 1992. (Publ. AL-SR-1992-0005)
37. **Presson, R. G., Jr., K. R. Kirk, K. A. Haselby, J. H. Linehan, S. Zaleski and W. W. Wagner, Jr.** Fate of air emboli in the pulmonary circulation. *J. Appl. Physiol*. 67: 1898–1902, 1989.
38. **Presson, R. G., Jr., K. R. Kirk, K. A. Haselby, and W. W. Wagner, Jr.** Effect of ventilation with soluble and diffusible gases on the size of air emboli. *J. Appl. Physiol*. 70: 1068–1074, 1991.
39. **Sergysels, R., N. Jasper, L. Delaunois, H. K. Chang, and R. R. Martin.** Effect of ventilation with different gas mixtures on experimental lung air embolism. *Respir. Physiol*. 34: 329–343, 1978.
40. **Shirai, M., K. Sada, and I. Ninomiya.** Diameter and flow velocity changes in small pulmonary vessels due to microembolization. *J. Appl. Physiol*. 65: 288–296, 1988.
41. **Steffey, E. P., B. H. Johnson, and E. I. D. Eger.** Nitrous oxide intensifies the pulmonary arterial pressure response to venous injection of carbon dioxide in the dog. *Anesthesiology* 52: 52–55, 1980.
42. **Van-Liew, H. D., and M. E. Burkard.** Bubbles in circulating blood: stabilization and simulations of cyclic changes of size and content. *J. Appl. Physiol*. 79: 1379–1385, 1995.
43. **Vann, R. D., and E. D. Thalmann.** Decompression physiology and practice. In: *The Physiology and Medicine of Diving* (4th ed.), edited by P. B. Bennett and D. H. Elliott. London: Saunders, 1993, p. 376–432.
44. **Verstappen, F. T., J. A. Bernards, and A. F. Kreuzer.** Effects of pulmonary gas embolism on circulation and respiration in the dog. II. Effects on respiration. *Pflügers Arch*. 368: 599–604, 1977.
45. **Verstappen, F. T., J. A. Bernards, and F. Kreuzer.** Effects of pulmonary gas embolism on circulation and respiration in the dog. III. Excretion of venous gas bubbles by the lung. *Pflügers Arch*. 370: 67–70, 1977.
46. **Vik, A., A. O. Brubakk, T. R. Hennessy, B. M. Jenssen, M. Ekker, and S. A. Slordahl.** Venous air embolism in swine: transport of gas bubbles through the pulmonary circulation. *J. Appl. Physiol*. 69: 237–244, 1990.
47. **Waligora, J. M., D. J. Horrigan, Jr., and J. Conklin.** The effect of extended O_2 prebreathing on altitude decompression sickness and venous gas bubbles. *Aviat. Space Environ. Med*. 58, *Suppl*.: A110–A112, 1987.
48. **Walmrath, D., R. Konig, C. Ernst, H. Bruckner, F. Grimminger, and W. Seeger.** Ventilation-perfusion relationships in isolated blood-free perfused rabbit lungs. *J. Appl. Physiol*. 72: 374–382, 1992.
49. **Walther, S. M., K. B. Domino, R. W. Glenny, and M. P. Hlastala.** Pulmonary blood flow distribution in sheep: effects of anesthesia, mechanical ventilation, and change in posture. *Anesthesiology* 87: 335–342, 1997.
50. **Walther, S. M., K. B. Domino, R. W. Glenny, N. L. Polissar, and M. P. Hlastala.** Pulmonary blood flow distribution has a hilar-to-peripheral gradient in awake, prone sheep. *J. Appl. Physiol*. 82: 678–685, 1997.
51. **Yen, R. T., and Y. C. Fung.** Effect of velocity distribution on red cell distribution in capillary blood vessels. *Am. J. Physiol*. 235 (*Heart Circ. Physiol*. 4): H251–H257, 1978.